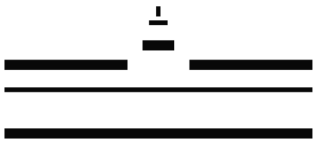

Master Thesis:

Comparison of Jet Quenching mechanisms in heavy ion collisions

Supervisors:
Prof. Dr. M. Klasen
Prof. Dr. J. Wessels

January 22, 2015

Semir Vrana

Contents

1 Introduction

Quarks are the fundamental building blocks of all known matter. Due to the so called color-confinement it is not possible to observe them as free particles, but from the theory of the strong interactions, quantum chromodynamics (QCD), one expects the strong coupling constant to decrease at high energies, respectively high temperatures, leading to the assumption that quarks are asymptotically free at those energies. The expected phase diagram of QCD is shown in figure 2.

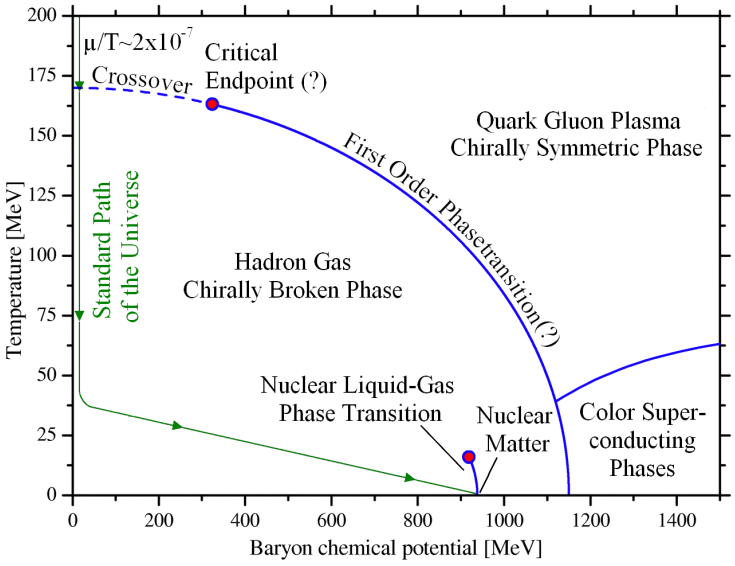

Figure 2: The QCD phase diagram. Taken from [1].

The state of free quarks is called quark-gluon-plasma (QGP) and was according to the standard model of cosmology formed 10^{-6} seconds after the big bang. Since the universe is expanding, it cooled down and the QGP hadronized after 10^{-4} seconds [17].
Another field where QGPs can occur, even at the current temperature of the universe, are neutron stars. In ordinary stars the gravitational pressure acting towards the inside of the star is balanced by a radiation pressure due to nuclear reactions inside of the star. At the end of the lifetime of a star, the decreasing rate of nuclear reactions inside the star cannot stop it anymore from collapsing due to the gravitational pressure and the star starts collapsing. This final collapse is either stopped by the Fermi pressure of the electrons leading to White Dwarfs or by the Fermi pressure of the neutrons, which results in neutron stars or even black holes, if the initial star was very massive. It is possible that the core of a neutron star consists of a QGP [17].

When reaching high energies, hadrons should deconfine again and form a QGP. In experiments at the LHC in CERN one collides two lead ions at a center-of-mass-energy of 2760 GeV hoping to create such a QGP and learn more about it.
One effect where the formation of a QGP shows is called "jet quenching", where in a collision of two heavy ions, jets are formed that have lower energy to corresponding jets in Proton-Proton-Collisions since former jets have to pass through the plasma and will thus interact with it.
In this thesis, two models for jet quenching will be discussed and the resulting suppression of jets will be compared to each other and to measurements from ALICE at LHC.

2 Perturbative QCD

When simulating scattering events at high energy colliders to investigate jet quenching, one has to consider scatterings of the type $pp(\mathrm{PbPb}) \rightarrow \mathrm{Jets} + \mathrm{X}$, where X stands for anything but jets. Jets will be defined later.
One difficulty in the theoretical description of this processes is that protons and especially lead nuclei are compound objects whose interactions are much more complicated than the interactions of the quarks that build them up. This problem will be solved by separating these interactions into a short-range and a long-range part using the factorization theorem so that it is only necessary to be able to calculate the cross sections for the interactions of quarks and gluon using QCD and add long-range physics via universal parton distribution functions.

2.1 Quantum Chromodynamics

Quantum Chromodynamics (QCD) is the theory of the strong interaction between quarks and gluons. It describes the confinement of quarks into hadrons as well as hadron collisions at high energy. The theory is based on the $SU(3)_c$ group of unitary matrices with unit determinant as a gauge group.
Additionally, the theory has a global $U(1)$ symmetry which leads to the conservation of baryon number and, when only considering the lightest three quarks, it has an approximate $SU(3)_f$ symmetry of flavor which is explicitly broken by the quark masses and by electromagnetic interactions due to differing electric charges.

The Lagrangian of QCD is given as [2]

$$\mathcal{L}_{\text{QCD}} = \bar{\mathrm{q}}_f^i \mathrm{i}\gamma^\mu (D_\mu)_{ij} \mathrm{q}_f^j - m_f \bar{\mathrm{q}}_f^i q_f^i - \frac{1}{4} F_{\mu\nu}^a F^{a\mu\nu}. \tag{2.1}$$

The q_f^i are the quark fields where $i, j \in \{1, 2, 3\}$ are color indices and f is a flavor index for the six different quark flavors. $(D_\mu)_{ij} = \partial_\mu \delta_{ij} - \mathrm{i} g A_\mu^a (T^a)_{ij}$ is the covariant derivative, where g is the strong coupling constant, A_μ^a are the gluon fields and T^a are the generators of the $SU(3)_c$ group in the adjoint representation. m_f labels the quark masses and is usually neglected in high energy collisions. $F_{\mu\nu}^a = \partial_\mu A_\nu^a - \partial_\nu A_\mu^a + g f^{abc} A_\mu^b A_\nu^c$ is the field strength tensor, where $a, b, c \in \{1, ..., 8\}$ are color indices and f^{abc} are the structure constants of the $su(3)$ Lie algebra. Summation over all doubly appearing indices is taken to be implicit. The color indices i, j are usually suppressed in the notation.
In the massless limit, $m_f = 0$, the symmetry of the Lagrangian extends $SU(N_f) \times SU(N_f)$ where one $SU(N_f)$ is generated by $N_f^2 - 1$ matrices T^a and the other by chiral $\gamma_5 \cdot T^a$ [3]. When quantizing the theory, one has to add a gauge fixing term $\mathcal{L}_{\text{gf}} = -(\partial^\mu A_\mu^a)^2/(2\xi)$ and a ghost term $\mathcal{L}_{\text{gh}} = (\partial_\mu \bar{c}_a)(\partial^\mu \delta_{ad} - g f_{abd} A_b^\mu) c_d$ [4] to the Lagrangian to prevent zero modes when solving for the Greens functions and to cancel unphysical degrees of freedom.

2.2 Running Coupling and Asymptotic Freedom

When calculating physical observables in quantum field theory, one finds that the occurring integrals can be divergent and thus have to be regularized to get finite results [5]. Usually this involves the introduction of a dimensional yet unphysical scale parameter μ so that an observable $\mathcal{A}$ calculated this way will also depend on it, i.e. $\mathcal{A} = \mathcal{A}(\alpha_s, \mu)$. Here, $\alpha_s = g^2/(4\pi)$ is the strong coupling constant. Since physical quantities cannot depend on a non-physical scale one has to make the strong coupling constant also scale dependent to compensate this. This is usually formulated as a renormalization group equation

$$\mu \frac{\mathrm{d}\mathcal{A}}{\mathrm{d}\mu} (\alpha_s(\mu), \mu) = 0. \tag{2.2}$$

In QCD, one obtains at leading order that it must have the form [2]

$$\alpha_s(Q^2) = \frac{\alpha_s(M_Z^2)}{1 + \frac{11 C_A - 4 T_R n_f}{24\pi^2} \alpha_s(M_Z^2) \ln \frac{Q^2}{M_Z^2} + \mathcal{O}(\alpha_s^2)}, \tag{2.3}$$

to achieve this, where $\alpha_s(M_Z^2)$ is the value of the strong coupling at the mass scale of the Z-boson and C_A and T_R are the Casimirs of $SU(3)$. The coupling strength is now depending on the energy scale of the process. This is called "running coupling". One can deduce that the coupling is strong if the scale is low and if the scale is high the interaction gets weaker. This phenomenon is called asymptotic freedom.
Since μ is non-physical, there is a priori no right value for it. Usually, one chooses μ to be equal to a characteristic scale in process, e.g. the momentum of the exchanged virtual particle in a leading order process, and varies this scale to get an error estimate.
Asymptotic freedom leads also to the assumption that at high energy scales quarks will approximately behave like free particles instead of being bound into hadrons and hence that perturbation theory becomes more trustworthy at higher scales.

2.3 Parton model and Factorization

In the parton model, the collisions cross section for hadrons A and B is calculated using the formula [4]

$$\sigma_{AB}(p,p') = \sum_{\text{partons } i,j} \int_0^1 \mathrm{d}x \int_0^1 \mathrm{d}x' \hat{\sigma}_{ij}(xp, x'p', \mu_F)\phi_{i/A}(x,\mu_F)\phi_{j/B}(x',\mu_F), \tag{2.4}$$

where $\hat{\sigma}_{ij}$ is the cross section at parton level and $\phi_{i/h}$ is the parton density function (PDF) giving the probability to find a parton i carrying a momentum fraction xp, $x \in [0,1]$, in the hadron h. μ_F is the factorization scale which will be discussed later. This can be thought of as the joint probability of three uncorrelated events.
The factorization theorem has yet to be proved for jet-production in hadron-collisions. So far, it has just been proved for deeply-inelastic scatterings and Drell-Yan-processes[1].
Following [4], one can get an insight into this theorem in the case of deeply-inelastic lepton hadron scattering. A nucleon with momentum p consists of a set of partons i in a state with momentum fractions $x_i p$, $x_i \in [0,1]$. Suppose that this state has a lifetime of $\tau > \tau_0 > 0$ in its rest frame where τ_0 is a lower bound of the lifetime. In the center of mass system, the lifetime is dilated, $\tau' = \tau\sqrt{(1-v^2)} \gg \tau$. Furthermore, because of Lorentz contraction, the nucleus will look like a flat disk in the rest frame. From the viewpoint of an electron that is colliding with the nucleus it is effectively frozen while the it passes.
According to the uncertainty principle the electron has to be as close as $\mathcal{O}(1/Q)$, $Q^2 = -q^2$,

[1] This are proton-proton-collisions where a quark and a antiquark produce a lepton-antilepton-pair.

to the parton to exchange a large momentum q^μ. Suppose that the nucleus is approximately spherical with a radius R_0 and the partons are evenly spread out over the nucleus. Then it will be suppressed by a geometrical factor

$$\frac{1/Q^2}{\pi {R_0}^2} \ll 1 \tag{2.5}$$

that another parton is close enough to take part in the scattering described above. Because of this, one may write the cross section as the probability of finding a parton in the nucleus with given momentum fraction times the cross section for the interaction.

2.4 Parton density functions and the DGLAP equation

The factorization scale μ_f in equation (2.4) arises due to the ambiguity in separating long range physics from short range physics. Only propagators that are off-shell by more than μ_f will contribute to the calculation of $\hat{\sigma}_{ij}$ [4]. The residual will be part of $\phi_{i/h}$. Since $\phi_{i/h}$ contains all the non-perturbative contributions to the process it cannot be calculated using perturbation theory but has to be measured. The PDFs are only depending on μ_f and the particular hadron that is colliding but not on the hard-scattering process.
The factorization scale like the renormalization scale is an artificial one, meaning that physical quantities cannot depend on it. This fact can be exploited using a renormalization group equation [4], giving

$$\mu_f \frac{\mathrm{d}\phi_{i/h}}{\mathrm{d}\mu_f}(x,\mu_f) = \frac{\alpha_s}{2\pi} \sum_{j=f,\bar{f},G} \int_x^1 \frac{\mathrm{d}\xi}{\xi} P_{ij}\left(x/\xi\right) \phi_{j/h}(\xi,\mu_f) + \mathcal{O}(\alpha_s^2), \tag{2.6}$$

where the integration kernel P_{ij} turns out to be the splitting function that will play a large role in parton showers, which will be discussed later. Using this formula, one can measure the PDFs at one scale μ_f und calculate them at another scale μ_f'.
The usual convention is to choose the factorization scale to be equal to the renormalization scale, such that $\mu_f = \mu = Q$.
Since protons consist of three valence quarks uud and vacuum fluctuations [19], one finds for the expectation values for up and down quarks in a proton

$$\langle N_u \rangle = \int_0^1 \mathrm{d}x(\phi_{u/p}(x) - \phi_{\bar{u}/p}(x)) = 2, \quad \langle N_d \rangle = \int_0^1 \mathrm{d}x(\phi_{d/p}(x) - \phi_{\bar{d}/p}(x)) = 1. \tag{2.7}$$

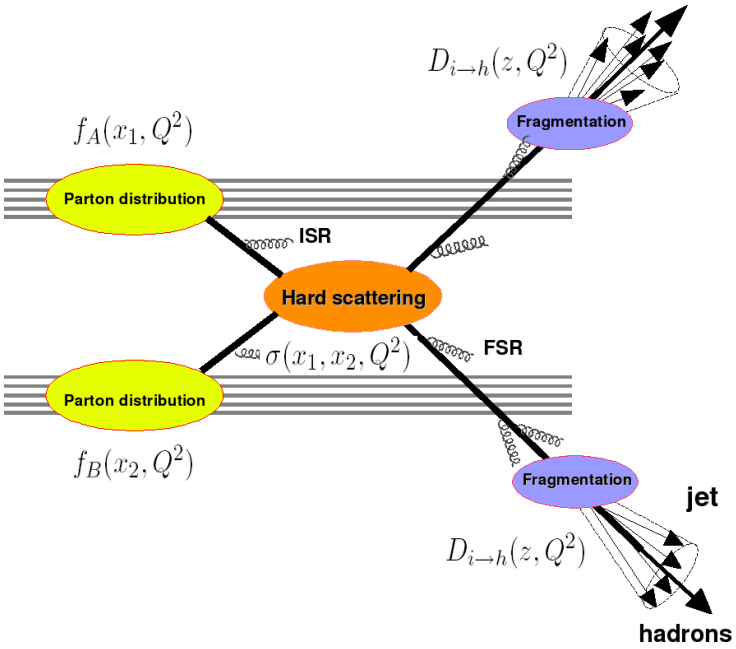

Figure 3: Schematic picture of a hadron hadron collision as it is calculated in perturbation theory. Two partons from the two hadron are reacting, emitting gluon radiation and finally fragmenting into hadrons. Taken from [6].

Furthermore, the sum of all parton momenta must give the proton momentum, hence

$$\left\langle \sum_{\text{partons } i} x_i \right\rangle = \int_0^1 \mathrm{d}x\, x \left(\sum_q \phi_{q/h}(x) + \sum_{\bar{q}} \phi_{\bar{q}/h}(x) + \phi_{g/h}(x) \right) = 1. \tag{2.8}$$

3 Parton shower and event generation

The processes calculated in perturbation theory usually do not resemble the events at high energy colliders. While in perturbation theory the incoming particles interact only via a few vertices leading to the creation of a handful of particles, in colliders these particles are interacting a lot more and run through a cascade of splittings and decays as shown in figure 3. This motivates the concepts of parton showers where the splitting of a parton into two partons is described via the before mentioned splitting functions. These splittings are done until a low non-perturbative energy scale is reached where the partons hadronize.

3.1 Splitting functions

Splitting functions are the fundamental building block of a parton shower. To define them, one considers a process where two partons interact producing three partons. One can think of this process as a $2 \to 2$ process, where one of the outgoing partons emits a further parton. In the collinear limit of this splitting the cross section can generally be written as

$$\mathrm{d}\sigma_{n+1} = \sigma_n \sum_{\text{partons},i} \frac{\alpha_s}{2\pi} \frac{\mathrm{d}\theta^2}{\theta^2} \mathrm{d}z \, P_{ji}(z,\phi)\mathrm{d}\phi,$$

where $P_{ji}(z)$ is the splitting function, depending on the energy fraction z that the outgoing parton gets [8]. The splitting functions do not depend on the process that is considered. Since the cross section is a measure for the probability of a reaction to happen, the splitting function can be interpreted as a probability for a branching to occur.
Instead of using θ^2, one can also use any other variable proportional to θ^2 to parametrize the phase space, e.g. the virtuality[2] of the internal quark line $q^2 = z(1-z)\theta^2 E^2$, giving $\mathrm{d}\theta^2/\theta^2 = \mathrm{d}q^2/q^2$.
The different splitting functions have the following form

$$P_{qq}(z) = C_F \frac{1+z^2}{1-z}, \qquad P_{gq}(z) = C_F \frac{1+(1-z)^2}{z}, \tag{3.1}$$

$$P_{gg}(z) = C_A \frac{z^4+1+(1-z)^4}{z(1-z)}, \qquad P_{qg}(z) = P_{\bar{q}g}(z) = T_R(z^2+(1-z)^2), \tag{3.2}$$

where C_A, C_F and T_R are the Casimirs of $SU(3)$ [2]. The splitting functions P_{qq}, P_{gq}, P_{gg} and P_{qg} correspond to the splitting $q \to qg$, $q \to gq$, $g \to gg$ and $g \to q\overline{q}$ respectively.
From the splitting function, one can now obtain a well-defined probability distribution for a splitting to occur. In order to do that, one has to handle the divergencies of the splitting functions. Since one cannot distinguish a collinear pair of partons from a single parton with the same momentum and quantum numbers, the infinite probability connected to this splitting has no physical meaning and one can simply remove it by introducing a cut-off Q_0 as a resolution criterion. The distribution for the splitting of a parton i between q^2 and

[2]The virtuality Q is defined as the mass a virtual particle would have according to the energy-mass relation $Q^2 = E^2 - \vec{p}^2$.

$q^2 + \mathrm{d}q^2$ can then be written as

$$\mathrm{d}\mathcal{P}_i = \frac{\alpha_s}{2\pi}\frac{\mathrm{d}q^2}{q^2}\int\limits_{Q_0^2/q^2}^{1-Q_0^2/q^2}\mathrm{d}z\, P_{ji}(z).$$

This gives the probability distribution for all emissions. But for a parton shower, one is only interested in the probability distribution of the first branching since the following splittings can be obtained by iterating such branchings.
Let $\Delta_i(Q^2, q^2)$ be the probability for no splittings to occur between the scales q^2 and Q^2. Then its derivative $\mathrm{d}\Delta_i/\mathrm{d}q^2$ gives the probability distribution for a splitting at q^2. This can be written as

$$\frac{\mathrm{d}\Delta_i(Q^2, q^2)}{\mathrm{d}q^2} = \Delta_i(Q^2, q^2)\frac{\mathrm{d}\mathcal{P}_i}{\mathrm{d}q^2}, \tag{3.3}$$

since Δ_i gives the probability that the parton has not already branched between q^2 and Q^2 which has to be multiplied by the probability that the splitting occurs at q^2. The differential equation (3.3) has the solution [8]

$$\Delta_i(Q^2, q^2) = \exp\left(-\int_{q^2}^{Q^2}\frac{\mathrm{d}k^2}{k^2}\frac{\alpha_s}{2\pi}\int\limits_{Q_0^2/k^2}^{1-Q_0^2/k^2}\mathrm{d}z\, P_{ji}(z)\right). \tag{3.4}$$

For $q^2 = Q_0^2$ this is the so-called Sudakov form factor which gives the probability for a parton not to split between the hard scale Q^2 and the infrared cut-off Q_0^2.

3.2 Vacuum parton shower

Using the above derived probability distribution, one can simulate a sequence of parton branchings in the vacuum [8]. The generation of splittings in the presence of strongly interacting matter will be discussed later.
One generates a uniformly distributed random number $\rho \in [0, 1]$ and solves the equation $\Delta_i(Q^2, q^2) = \rho$ for q^2. If the obtained q^2 is larger than Q^2, a branching at this scale is generated and if it is smaller, the evolution stops. The energy fraction z of the emitted parton is chosen with respect to its probability distribution $P_{ji}(z)$.
As mentioned before, there are ambiguities in the choice of q^2 and z that would give the

same results in the collinear limit but give different extrapolations in the other regions of the phase space.
So far, this algorithm is only valid in the collinear region, since the soft divergencies were not taken into account.

3.2.1 Soft gluon emission

Apart from the collinear divergence, QCD matrix elements can also be divergent in the soft limit. In this case, the factorization happens at the amplitude level which means that one cannot see these processes as $2 \to 2$ diagrams with an additional emission but as the whole process emitting the gluon so that it seems as if it is not possible to describe these emissions as the evolution of a parton that emits the gluon [8].
It can be shown that a wide angle gluon would get a wavelength that is larger than the distance of the two outgoing partons can get during the lifetime of the partons so that the gluon cannot resolve the color structure inside the event[3]. These gluons are emitted as if they were emitted by the parent parton with on shell momentum.
This is automatically included in the collinear parton shower algorithm if one takes the opening angle of the emission as the evolution scale.

3.2.2 Initial state shower

The branching of partons is not restricted to after the hard event has taken place. So for a realistic description of a collision, one has to take into account that the incoming partons can emit additional partons and lose energy by doing so.
Instead of following all the emitted partons to find the one that is taking part in the hard process, event generators start by selecting the hard process and describe the initial state parton shower by a backward evolution.
First, the longitudinal momentum fraction x_1 and x_2 and the evolution scale are chosen following the PDF at the hard scale and the constraint $x_1 x_2 s = \hat{s}$. During the backward evolution these partons gain energy with each splitting until the scale reaches the infrared

[3]This is the analogue to the Chudakov effect in QED, where a wide-angle photon with a wavelength larger than the distance of an outgoing $e\bar{e}$-pair cannot resolve the charge inside the $e\bar{e}$-pair and thus would see no charge. Because of this such a process is strongly suppressed.

cut off. For the splitting probability one gets the modified Sudakov form factor [8]

$$\Delta_i(Q^2, q^2; x) = \exp\left(- \int_{q^2}^{Q^2} \frac{\mathrm{d}k^2}{k^2} \frac{\alpha_s}{2\pi} \int_{Q_0^2/k^2}^{1-Q_0^2/k^2} \mathrm{d}z \, P_{ji}(z) \frac{x/z\phi_j(x/z, k^2)}{x\phi_i(x, k^2)} \right), \tag{3.5}$$

where ϕ_i are PDFs.

3.3 Hadronization

After the parton shower has reached the infrared cut off, one ends up with a set of partons that cannot be observed in any experiment. Instead, the partons have to be bound to hadrons which can be observed. There is no first principle solution to achieve this [2], so phenomenological models are used instead. In the following, the Lund string model will be discussed.

In Lattice QCD calculations, one finds the attracting potential between two quarks to be $V(r) = \kappa r$, where the string constant has the value $\kappa \approx 0.2\,\mathrm{GeV}^2$ [8]. The potential acts like a string between the quarks. At short distances, one gets an additional Coulomb term $\propto r^{-1}$ which is neglected in the Lund model.

In a $q\bar{q}$ two-parton event, the distance inbetween these quarks tends to grow and so does the potential energy until the energy reaches that of hadron masses where it is energetically favorable for the string to create a $q'\bar{q}'$ pair and split into the two substrings $q\bar{q}'$ and $q'\bar{q}$ as in figure 4 shown. The pair $q'\bar{q}'$ can be thought of as products of vacuum fluctuations.

These substrings move apart and if the invariant mass is large enough, they can break again. At the end of the process, a set of $n-1$ new $q_i\bar{q}_i$ pairs is produced that fragments into n primary hadrons that can decay further.

There is no natural ordering for the splitting of the strings to happen. So one can start from the "left" quark as well as from the "right" anti-quark and iterate splittings toward the other ends. Both ways should lead to the same hadronic state. For the production of one hadron between the vertices 1 and 2 this reads as the condition for the probabilities $\mathcal{P}(1)\mathcal{P}(1 \to 2) = \mathcal{P}(2)\mathcal{P}(2 \to 1)$ where $\mathcal{P}(i)$ is the probability to reach the vertex i from "left"/"right" and $\mathcal{P}(i \to j)$ the probability to take the step from vertex i to j. This condition can be fulfilled with a fragmentation function [8]

$$f(z) \propto \frac{(1-z)^a}{z} \exp\left(-\frac{bm_\perp^2}{z}\right)$$

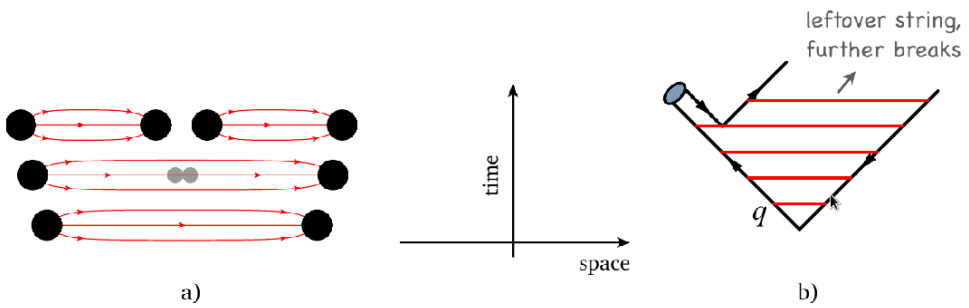

Figure 4: Schematic picture of the hadronization process. a) shows the breaking of a string into two substrings by quark pair production and b) shows the spatio-temporal progress of the hadronization. Taken from [2].

where $m_\perp^2 = m^2 + p_x^2 + p_y^2 = \kappa^2((\Delta z)^2 - (\Delta t)^2)$ is the transverse mass of the produced hadron where Δz is the distance of the quarks along the string and Δt is and a, b are free parameters.

In order to give transverse momentum to the hadron, the $q\bar{q}$ pair has to be produced at a certain distance. However, since flavor is locally conserved [12], the $q\bar{q}$ pair has to be produced in one point and tunnel this distance. The tunnel probability is proportional to

$$\exp\left(-\frac{\pi m_\perp^2}{\kappa}\right) = \exp\left(-\frac{\pi m^2}{\kappa}\right)\exp\left(-\frac{\pi p_\perp^2}{\kappa}\right). \tag{3.6}$$

Here, m and $p_\perp$ respectively are the mass and the transverse momentum of the produced quark. This implies a suppression of heavy quarks.

After the flavors q_{i-1} and $\bar{q}_i$ are selected, they have to be assigned to a hadron multiplet that is classified by the quantum numbers spin S and angular momentum L.

For mesons, this quantum numbers are chosen randomly from distributions depending on the flavors [12]. This cannot be generalized to include baryons, since baryons consist of three quarks. One way is instead to assume that during the string breaking not only quark anti-quark pairs, but also diquark anti-diquark pairs in a triplet-antitriplet representation are produced, which can form baryons. Since there is a large uncertainty on the masses of bound quark states, one cannot use formula (3.6). From experiment, one finds for the probability of diquarks $P(qq)/P(q) \approx 0.065$ [13]. These diquarks can then be used to build up baryons the same way as mesons are build.

4 Jet Clustering

While calculations in perturbation theory usually have two or three partons in the final state, a measurement in collider experiments as well as the output in event generators consists of much larger multiplicities due to branching, hadronization and decays of unstable particles.
For a better understanding, one is interested to rediscover the properties of the outcoming partons in this output. This leads to the definition of Jets.
A jet definition consists of a jet algorithm that decides which particles belong to the same jet and it consists of a recombination scheme that gives the jet a well-defined momentum. Every jet definition should meet the following conditions ("snowmass accord")[7]

1. Simple to implement in an experimental analysis;
2. Simple to implement in the theoretical calculation;
3. Defined at any order in perturbation theory;
4. Yields finite cross sections at any order in perturbation theory;
5. Yields a cross section that is relatively insensitive to hadronization.

4.1 Jet algorithms

There are two main classes of algorithms used to define a Jet. In cone algorithms, one basically takes an initial seed particle and defines a cone of a given radius around it. Every particle inside the cone belongs to this jet. In sequential recombination algorithms, two particles that are close in some sense are recombined into a pseudojet, i.e. a jet-like object. This is repeated until a break condition is fulfilled. The remaining pseudojets are then called jets.

4.1.1 Cone algorithms

In iterative cone algorithms, one takes an initial seed particle i, usually the hardest, and sums the momenta of all particles j inside a cone of radius R around i in azimuthal angle

ϕ and (pseudo-) rapidity[4] y. So all particles j with

$$\Delta R_{ij}^2 := (y_i - y_j)^2 + (\phi_i - \phi_j)^2 < R^2 \tag{4.1}$$

are inside the cone. The sum of the momenta defines the new direction for the cone and one repeats this procedure until the direction of the cone is stable. This defines one jet.
To prevent particles from ending up in more than one jet, all particles inside an once found jet are removed from the particle list. The hardest remaining particle defines the initial direction of the second cone. This is continued until no remaining particle has a transverse momentum above a given $p_{T,\text{cut}}$.
One requirement jet algorithms have to fulfill is that they have to be infrared safe, i.e. adding any number of soft particles or any number of collinear splittings of existing particles should not change any observable. If this is the case, jet cross sections are finite at any order in perturbation theory and any corrections due to non-perturbative effects are suppressed by powers of jet momenta [8].
In the cone algorithm one chooses the hardest particle as a seed for the algorithm but in the case of collinear or soft emissions, this does not have to be the case anymore. Therefore another particle could be the seed and the output of the algorithm would differ. Hence the algorithm is not infrared and collinear safe.
One solution to this problem would be to use seedless cone algorithms that are not finding the stable cones consecutively using a seed particle but finding all stable cones at once [7]. One implementation that uses this technique is SIScone [9].
Another approach is to use sequential recombination algorithms that are thus presented in the next section.

4.1.2 Sequential recombination jet algorithms

In sequential recombination algorithms, instead of starting from the hardest particles, one starts from the closest pair and recombines them to pseudojets until all distances are above a given distance cut.

[4]The pseudo-rapidity is defined as $\eta = -\ln\tan(\theta/2)$ where θ is the angle between the three-momentum of the particle and the beam axis. For massless particles the rapidity and the pseudo rapidity are the same.

For the distance measure between two particles i and j one defines

$$d_{ij} = \min(p_{T,i}^{2a}, p_{T,j}^{2a}) \frac{\Delta R_{ij}^2}{R^2}, \tag{4.2}$$

where as in the cone algorithm $\Delta R^2 = \Delta y^2 + \Delta\phi^2$ and R is a given Radius parameter. One further defines a distance between particle i and the incoming particle beams as $d_{iB} = p_{T,i}^{2a}$. All these distance measures are invariant under longitudinal Lorentz boosts along the beam axis. a is an integer that distinguishes between different algorithms. $a = 1$ corresponds to the k_T-algorithm, $a = 0$ is the Cambridge/Aachen-algorithm and $a = -1$ gives the anti-k_T-algorithm.
The algorithm follows the steps [10]

1. Calculate all d_{ij} and d_{iB}
2. Find the minimum $d_{\min}$ of all d_{ij}, d_{iB}.
3. If $d_{\min} = d_{ij}$ recombine the particles i and j and if $d_{\min} = d_{iB}$ declare i to be a jet and remove it from the list.
4. Repeat until no particles are left.

This algorithm is infrared and collinear safe since those kinds of emissions will be recombined directly at the start of the clustering.
By a naive approach it would take $\mathcal{O}(N^3)$ steps to cluster N particles to a jet, the matrix d_{ij} has $\mathcal{O}(N^2)$ entries that one has to take into account for the minimum and one has to find the minimum $\mathcal{O}(N)$ times. Modern algorithms [10] are able to do the clustering in $\mathcal{O}(N \ln N)$.
In figure 5 the different jet algorithms are compared.

4.2 Recombination schemes

When recombining particles to jets, there are different ways to assign a momentum to it [10]. The simplest procedure is the E-sheme where all particle momenta are simply added.

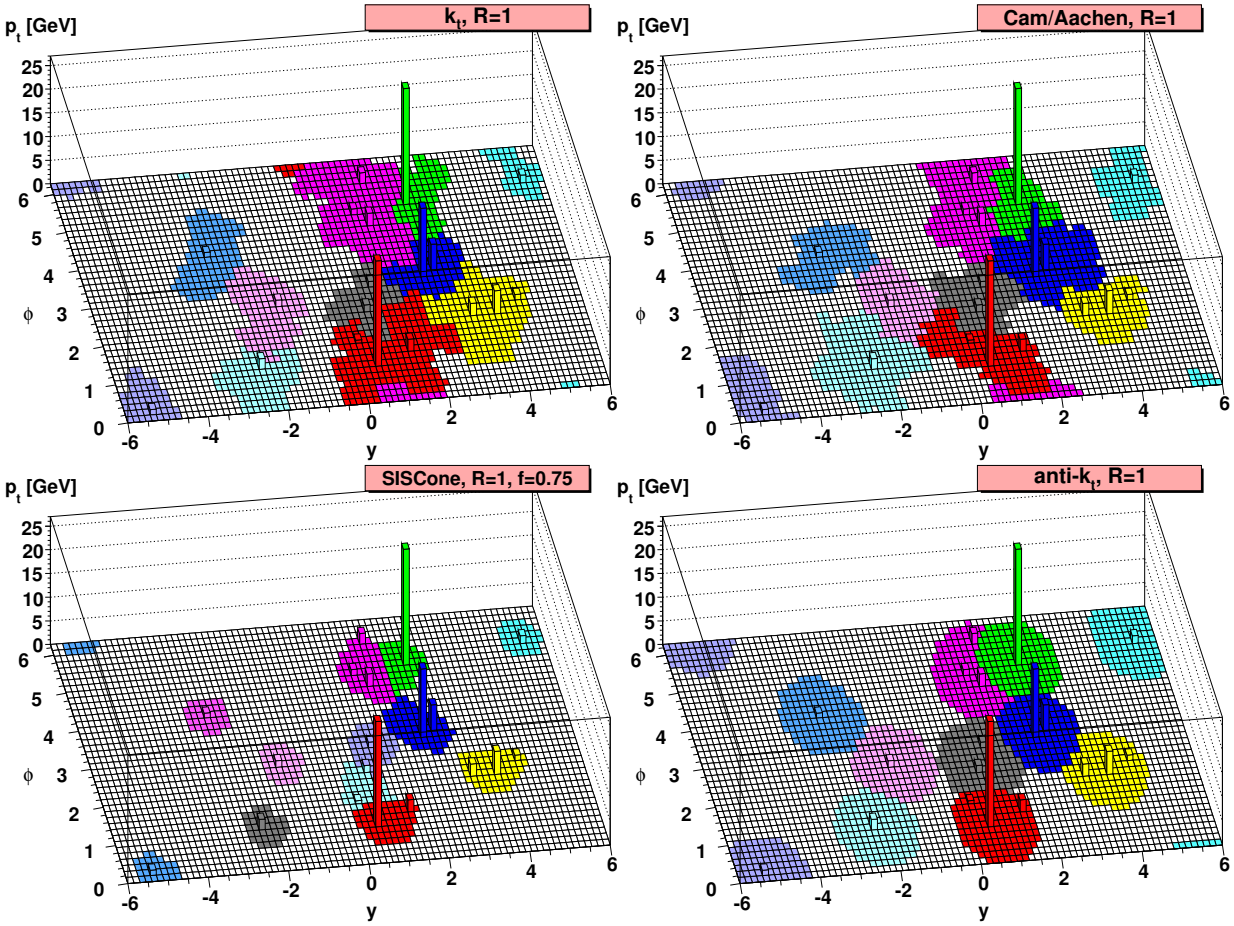

Figure 5: The resulting jet areas from the different jet algorithms. Partons that are in the shaded areas where clustered to the corresponding jet. It can be seen that the shape of the areas from the anti-k_T-algorithm have the best resemblance of cones. Taken from [7].

Other possibilities are the p_T and the p_T^2-scheme. In the p_T- and p_T^2-scheme one defines

$$p_{T,\text{jet}} = \sum_i p_{T,i}, \tag{4.3}$$

$$y_{\text{jet}} = \frac{\sum_i w_i y_i}{\sum_i w_i}, \tag{4.4}$$

$$\phi_{\text{jet}} = \frac{\sum_i w_i \phi_i}{\sum_i w_i}, \tag{4.5}$$

where $w_i = p_{T,i}$ for the p_T-scheme and $w_i = p_{T,i}^2$ for the p_T^2-scheme.

5 Quark-Gluon-Plasma

In this section, general properties of the QGP in a heavy ion collision will be discussed that will later be used to describe jet quenching.

5.1 Relativistic gas

Due to asymptotic freedom, one can assume that the QGP behaves as a free, relativistic gas. All its thermodynamic properties follow from the grand-canonical partition sum [14]

$$\Xi(T,V,\mu) = \sum_{\text{all states}} \exp\left(-\beta\left(E_{\text{tot}} - \mu N\right)\right), \tag{5.1}$$

$$= \sum_{n(\vec{\nu})} \exp\left(-\beta \sum_{\{n(\vec{\nu})\}} n(\vec{\nu})\left(E(\vec{\nu}) - \mu N\right)\right), \tag{5.2}$$

$$= \sum_{n(\vec{\nu})} \prod_{\vec{\nu}} \left[\exp\left(-\beta\left(E(\vec{\nu}) - \mu\right)\right)\right]^{n(\vec{\nu})}, \tag{5.3}$$

$$= \prod_{\vec{\nu}} \sum_{n(\vec{\nu})=0}^{\substack{\infty \text{ if bosons} \\ 1 \text{ if fermions}}} \left[\exp\left(-\beta\left(E(\vec{\nu}) - \mu\right)\right)\right]^{n(\vec{\nu})}, \tag{5.4}$$

$$= \prod_{\vec{\nu}} \frac{1}{1 \pm \exp\left(-\beta\left(E(\vec{\nu}) - \mu\right)\right)}. \tag{5.5}$$

Here, $n(\vec{\nu})$ is the occupation number and $E(\vec{\nu})$ is the one particle energy labeled by a set of quantum numbers $\vec{\nu}$. μ is the chemical potential and $\beta = 1/T$ the inverse temperature[5].

[5] In units where $k_B = 1$.

In the case of the bosons, (5.5) is the geometric sum formula. The plus sign in (5.5) applies to fermions and the minus sign to bosons. For the more useful logarithm of Ξ, one gets

$$\ln \Xi(T, V, \mu) = \pm \sum_{\vec{\nu}} 1 \pm \exp\left(-\beta \left(E(\vec{\nu}) - \mu\right)\right). \tag{5.6}$$

In the case that the energy levels are continuous rather than discrete, one can generalize this formula to

$$\ln \Xi(T, V, \mu) = \pm \int \frac{\mathrm{d}^3 p \, \mathrm{d}^3 q}{(2\pi)^3} \left(1 \pm \exp\left(-\beta \left(E\left(\vec{\nu}\right) - \mu\right)\right)\right). \tag{5.7}$$

From this, one can derive the mean occupation number to be

$$\bar{n}(\vec{\nu}) = -\frac{\partial \ln \Xi}{\partial(\beta E)} = \frac{1}{\exp\left(\beta(E-\mu)\right) \pm 1} \tag{5.8}$$

where as before the plus sign applies to fermions and the minus sign to bosons. For a baryon-free ($\mu = 0$) QGP, one can write this as

$$\bar{n}(\vec{p}) = \frac{g_{g/q}}{\mathrm{e}^{\beta E} \pm 1} \qquad \text{with} \qquad E = \sqrt{\vec{p}^2 + m^2}, \tag{5.9}$$

where $g_{g/q}$ is the number of degrees of freedom for quarks respectively gluons. Quarks have n_f flavor, three colors and two spin degrees of freedom, therefore $g_q = g_{\bar{q}} = 6n_f$, while gluons have 8 degrees of freedom for their color and two for their polarizations giving $g_g = 16$. For massless particles, one can find the particle and energy density analytically to be

$$n_g = \frac{1}{V} \int \frac{\mathrm{d}^3 q \, \mathrm{d}^3 p}{(2\pi)^3} \bar{n}(\vec{p}) = \frac{g_g}{\pi^2} T^3 \zeta(3) \approx 1.2 \frac{g_g}{\pi^2} T^3, \tag{5.10}$$

$$n_q = \frac{1}{V} \int \frac{\mathrm{d}^3 q \, \mathrm{d}^3 p}{(2\pi)^3} \bar{n}(\vec{p}) = \frac{g_q}{\pi^2} T^3 d(3) \approx 0.9 \frac{g_q}{\pi^2} T^3, \tag{5.11}$$

$$\epsilon_g = \frac{1}{V} \int \frac{\mathrm{d}^3 q \, \mathrm{d}^3 p}{(2\pi)^3} p \bar{n}(\vec{p}) = \frac{3 g_g}{\pi^2} T^4 \zeta(4) = \frac{\pi^2 g_g}{30} T^4, \tag{5.12}$$

$$\epsilon_q = \epsilon_{\bar{q}} = \frac{1}{V} \int \frac{\mathrm{d}^3 q \, \mathrm{d}^3 p}{(2\pi)^3} p \bar{n}(\vec{p}) = \frac{3 g_q}{\pi^2} T^4 d(4) = \frac{7\pi^2 g_q}{240} T^4, \tag{5.13}$$

with

$$\zeta(\xi) = \int_0^\infty \mathrm{d}\alpha \, \frac{\alpha^{\xi-1}}{\mathrm{e}^\alpha - 1}, \tag{5.14}$$

$$d(\xi) = \int_0^\infty \mathrm{d}\alpha \, \frac{\alpha^{\xi-1}}{\mathrm{e}^\alpha + 1}. \tag{5.15}$$

For the mean energy per particle, one gets then $\langle E_q \rangle = \epsilon_q / n_q \approx 3.2T$ and $\langle E_g \rangle \approx 2.7T$.

5.2 Relativistic hydrodynamics

After the collision of two heavy ions, the created QGP expands in all directions and cools down. This process can be described via relativistic hydrodynamics [15].
In order to apply hydrodynamics, one has to assume a local thermodynamic equilibrium, i.e. that for each point a neighborhood exists where this holds.
All thermodynamic properties will be defined in the fluid rest frame, i.e. the frame where all momentum components vanish. Due to local equilibrium the fluid will be isotropic in its fluid rest frame.
The velocity $\vec{v}$ of a fluid element is defined as the velocity of its rest frame with respect to the laboratory frame. The velocity 4-vector can then be defined to be $u^\mu = (\gamma, \gamma\vec{v})$ where $\gamma = (1 - v^2)^{-1/2}$. The continuity equation for the baryon density n can the be written as $\partial_\mu (n u^\mu) = 0$.
Energy and momentum conservation can be written as $\partial_\mu T^{\mu\nu} = 0$ where $T^{\mu\nu}$ is the energy-momentum-tensor. Due to isotropy one can write it in the fluid rest frame as

$$T_0 = \begin{pmatrix} \epsilon & 0 & 0 & 0 \\ 0 & P & 0 & 0 \\ 0 & 0 & P & 0 \\ 0 & 0 & 0 & P \end{pmatrix}, \tag{5.16}$$

where ϵ is the energy density and P thermodynamic pressure. This can be expressed through covariant vectors as $T^{\mu\nu} = (\epsilon + P) u^\mu u^\nu - P g^{\mu\nu}$ and since this is a covariant equation that holds in one frame, it is by construction true in all frames.
Besides the continuity equation and energy-momentum conservation, one needs an equation of state $f(\epsilon, P, n) = 0$ to form a complete set of equations.

5.3 Bjorken model

The Bjorken model describes the space-time evolution of a QGP using relativistic hydrodynamics to get a spatio-temporal picture of its state variables.
At the LHC, nuclei are colliding at an energy of 2.76 TeV per nucleus. This means that the nuclei are Lorentz contracted by a factor $\gamma \sim 10^3$. From the laboratory rest frame, the colliding nuclei look like flat disks.
In a collision, a large number of interacting particles is produced. If this interaction is strong enough, the system can reach a thermodynamic equilibrium. In the following, it is assumed that the system reaches an equilibrium at some point after the collision [15].
The z-axis is chosen to be the beam axis and the origin is chosen such that the collision takes place at $z = t = 0$. The initial conditions for the QGP are fixed at an initial proper time τ_0. A complete set of initial conditions consists of the fluid velocity, the energy density and the baryon density.
If t_0 is small enough v_x and v_y can be assumed to be zero, since the parton-parton-collisions occur on very short timescales and produce particles whose transversal momentum p_T is distributed isotropically over the transverse plane. Since no direction is preferred, averaging over a fluid element gives zero. The velocity can then be expressed as

$$u^\mu(\tau_0) = \frac{1}{\tau_0}(t, 0, 0, z) =: \frac{\tilde{x}^\mu}{\tau_0}. \tag{5.17}$$

Due to invariance under Lorentz boosts, $u^\mu = \tilde{x}^\mu/\tau$ hold for all proper times τ [16]. Using this, one can rewrite the momentum conservation equation $\partial_\mu T^{\mu\nu} = 0$ getting [17]

$$\frac{\mathrm{d}\epsilon}{\mathrm{d}\tau} = -\frac{\epsilon + P}{\tau}. \tag{5.18}$$

For an ultra-relativistic gas one can use the equation of state $P = \epsilon/3$ to get

$$\epsilon(\tau) = \epsilon(\tau_0) \left(\frac{\tau}{\tau_0}\right)^{-4/3}.$$

In a perfect fluid, the entropy density s is also conserved, giving the continuity equation $\partial_\mu(su^\mu) = 0$, which gives the differential equation

$$\frac{\mathrm{d}s}{\mathrm{d}\tau} = -\frac{s}{\tau}. \tag{5.19}$$

The equation is solved by

$$s(\tau) = s(\tau_0)\frac{\tau_0}{\tau}. \tag{5.20}$$

The time dependence of the temperature T can be obtained from (5.18) by writing

$$\frac{\mathrm{d}\epsilon}{\mathrm{d}\tau} = \frac{\mathrm{d}\epsilon}{\mathrm{d}P}\frac{\mathrm{d}P}{\mathrm{d}T}\frac{\mathrm{d}T}{\mathrm{d}\tau} = -\frac{\epsilon + P}{\tau} = -\frac{sT}{\tau}, \tag{5.21}$$

where the thermodynamic identity $E = TS - PV$ was used. With $s = \mathrm{d}P/\mathrm{d}T$ and $\mathrm{d}\epsilon/\mathrm{d}P = 1/v_s$, where v_s is the velocity of sound, one can rewrite this as [14]

$$\frac{1}{T}\frac{\mathrm{d}T}{\mathrm{d}\tau} = -\frac{v_s^2}{\tau}, \tag{5.22}$$

which is solved by

$$T(\tau) = T(\tau_0)\left(\frac{\tau_0}{\tau}\right)^{1/3}. \tag{5.23}$$

5.4 Glauber model

The Glauber model is used to calculate geometric quantities in heavy ion collisions [18]. In the optical limit it assumes that a collision of two nuclei can be described as independent interactions of the nucleons. It is further assumed that the nucleons move independently in the nuclei and that the size of the nuclei is large compared to the range of the nucleon-nucleon force.

Let two heavy ions A and B with relativistic velocities collide with impact parameter $\vec{b}$ as is illustrated in figure 6. The impact parameter $\vec{b}$ is defined as a two-dimensional vector corresponding the minimal perpendicular distance of the paths of the center of masses of the incoming nuclei. The probability of finding a nucleon at $\vec{s}$ in the transverse plane is then given by

$$T_{\mathrm{A}}(\vec{s}) = \int \mathrm{d}z_A\, \rho_A(\vec{s}, z_A), \tag{5.24}$$

where ρ_A is the probability to find a nucleon at $(\vec{s}, z_{\mathrm{A}})$ and the analogous expression holds for B. There are different possible normalizations for ρ_A, one can normalize it so that the integral over the whole space equals unity [18] or to be the number of nucleons in A

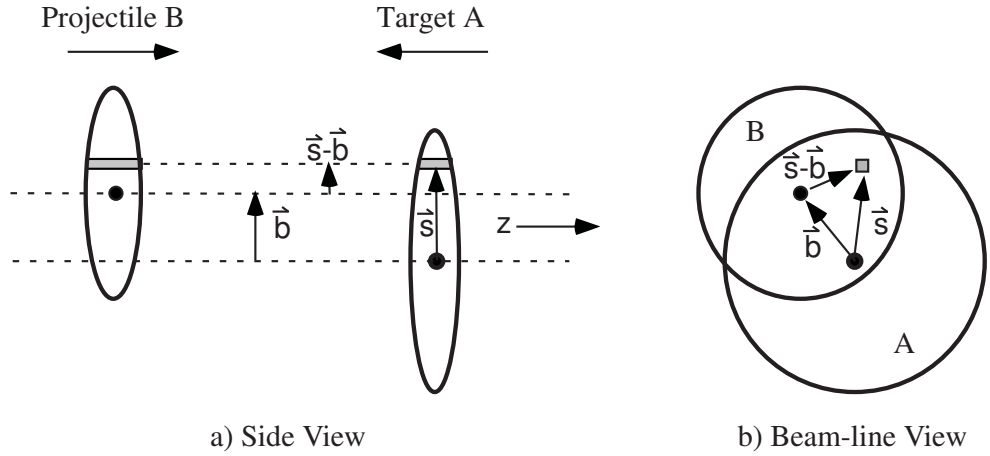

Figure 6: Schematic picture of the optical Glauber model. Taken from [18].

[14]. Usually ρ_A has the either the form of a sharp sphere, $\rho_A(r) \propto \theta(R-r)$, or of the Woods-Saxon-distribution

$$\rho_A(r) \propto \frac{1}{1+\exp(\frac{r-R}{d})}, \tag{5.25}$$

where R corresponds in both cases to the radius of the nucleus and d gives the width of the Woods-Saxon-distribution.
The probability that a nucleon from nucleus A meets a nucleon from B in an area element d^2s can then be written as the joint probability $T_\mathrm{A}(\vec{s})T_\mathrm{B}(\vec{s}-\vec{b})\mathrm{d}^2s$. Integrating this gives the so called thickness function

$$T_\mathrm{AB} = \int T_\mathrm{A}(\vec{s})T_\mathrm{B}(\vec{s}-\vec{b})\mathrm{d}^2s. \tag{5.26}$$

This can be interpreted as the effective overlap of the two nucleons. The probability for an interaction then is $T_\mathrm{AB}(\vec{b})\sigma_\mathrm{inel}^\mathrm{NN}$, where $\sigma_\mathrm{inel}^\mathrm{NN}$ is the inelastic nucleon-nucleon cross section. The probability of having n nucleon-nucleon interactions, where nuclei A and B consist respectively of A and B nucleons, can then be written as a binomial distribution

$$P(n,\vec{b}) = \binom{AB}{n}\left[T_\mathrm{AB}(\vec{b})\sigma_\mathrm{inel}^\mathrm{NN}\right]^n\left[1-T_\mathrm{AB}(\vec{b})\sigma_\mathrm{inel}^\mathrm{NN}\right]^{AB-n}. \tag{5.27}$$

This can be thought of as randomly drawing n out of AB possible interactions.
From this, one finds the probability for an interaction between A and B as the probability

that at least one nucleon-nucleon interaction happens at given impact parameter $\vec{b}$

$$p_{\text{inel}}^{\text{A+B}}(\vec{b}) = \sum_{n=1}^{AB} P(n,\vec{b}) = 1 - P(0,\vec{b}) = 1 - \left[1 - T_{\text{AB}}(\vec{b})\sigma_{\text{inel}}^{\text{NN}}\right]^{AB}. \tag{5.28}$$

This gives a probability distribution for the impact factor that can be used in Monte Carlo simulations.
Integration yields the total cross section

$$\sigma_{\text{inel}}^{\text{A+B}} = \int_0^\infty \mathrm{d}b\, 2\pi b \left(1 - \left[1 - T_{\text{AB}}(\vec{b})\sigma_{\text{inel}}^{\text{NN}}\right]^{AB}\right), \tag{5.29}$$

where it was assumed that the nuclei are not polarized so that the integrand is independent of the polar angle. For the mean number of binary nucleon-nucleon collisions one gets

$$N_{\text{coll}}(\vec{b}) = \sum_{n=1}^{AB} nP(n,\vec{b}) = AB\; T_{\text{AB}}(\vec{b})\sigma_{\text{inel}}^{\text{NN}}, \tag{5.30}$$

which is a standard result for binomial distributions. The number of participating nucleons is given by

$$\begin{aligned} N_{\text{part}}(\vec{b}) =& A \int T_{\text{A}}(\vec{s})\Big(1 - [1 - T_{\text{B}}(\vec{b} - \vec{s})]\Big)\mathrm{d}^2 s \\ &+ B \int T_{\text{B}}(\vec{b} - \vec{s})\Big(1 - [1 - T_{\text{A}}(\vec{s})]\Big)\mathrm{d}^2 s. \end{aligned} \tag{5.31}$$

The results from heavy ion experiments and also from simulations are usually classified by centrality c rather than the impact factor $b = |\vec{b}|$. The centrality is given as the percentage of events in a given impact factor range. For very central collisions, the geometric relation $c \approx \pi b^2/\sigma_{\text{inel}}$ holds.

6 Jet Quenching

After the collision of two protons, the outgoing partons are already in the vacuum and cannot interact further but only go through a parton shower and hadronize eventually. In the case of heavy ions, it is expected that a QGP is created around the scattering center and the outgoing partons have to propagate through this medium losing energy through collisions and medium induced radiation of gluons.

In the following, the two models that will be investigated later, are presented. Both JEWEL and PYQUEN modify the parton shower routine of the event generator PYTHIA [12].

6.1 JEWEL

In JEWEL [14, 20, 21, 22, 23], the medium is modeled as a collection of partons and the medium interactions of a jet are simply scatterings between the jet and the medium partons. The density and momentum distributions of the medium are those of massive quarks and gluons at the temperature T, cf. equation (5.8) with $\mu = 0$. The spatio-temporal evolution of the medium is guided by the Bjorken model. The mass of the scattering centers is fixed to $m_{\text{scatt}} = \mu_D(T)/\sqrt{2}$, where the Debye mass μ_D is approximated by $\mu_D \approx 3T$ in JEWEL. To define a parton shower inside a medium, one needs to have a spatio-temporal picture of it. A parton shower evolves down to a virtuality of Q_f and a time scale $\sim 1/Q_f$ in its rest frame. In the medium rest frame, it will be time-dilated to $\sim E/Q_f^2$. If the parton resulted from the branching of a parton at virtuality Q_i, it will have a lifetime of approximately

$$\tau \approx \frac{E}{Q_f^2} - \frac{E}{Q_i^2}. \tag{6.1}$$

For the elastic differential cross section, only the leading t-channel exchange is used,

$$\frac{\mathrm{d}\sigma^{\text{elas}}}{\mathrm{d}|t|} = \frac{\pi\alpha_s^2}{s^2} C_R \frac{s^2 + u^2}{|t|^2}, \tag{6.2}$$

where $C_R = 4/9$ for quark-quark, 1 for quark gluon and 9/4 for gluon-gluon scattering. The total cross section is obtained by integration and since the integrand is divergent for $|t| \to 0$, it has to be regularized.
With the probability

$$P_{\text{no scatt}}(\tau) = \exp\left(- \int_{t_p}^{t_p+\tau} \mathrm{d}t' \, \sigma_{\text{elas}}(\vec{r}(t'), t') n(\vec{r}(t'), t') \right) \tag{6.3}$$

the parton will not scatter elastically, where t_p is the partons production time. In the case of a homogeneous and static medium this reduces to

$$P_{\text{no scatt}}(\tau) = \mathrm{e}^{-\sigma^{\text{elas}} n \tau \beta}. \tag{6.4}$$

In analogy to the vacuum parton shower the probability for at least one splitting in $[t_p, t_p+\tau]$ is $1-P_{\text{no scatt}}(\tau)$ and the probability density for a splitting at a time τ_s is obtained by taking the derivative with respect to the proper time

$$p_s(\tau_s) = \frac{\mathrm{d}}{\mathrm{d}\tau}\left(1 - P_{\text{no scatt}}(\tau)\right)\Big|_{\tau=\tau_s} = \sigma_{\text{elas}} n \beta \mathrm{e}^{-\sigma^{\text{elas}} n \tau_s \beta}. \tag{6.5}$$

In the Monte Carlo simulation, one knows the virtuality of a parton from the previous branching. This is used to determine its lifetime according to equation (6.1). With a probability $1 - P_{\text{no scatt}}(\tau)$ the parton scatters at some time $\tau' < \tau$ at a medium parton. In this case the partons exchange momentum according to (6.2). It is then checked if another scattering is possible before splitting.
Inelastic scatterings are included by adding the inelastic cross section to (6.2), where one finds after a lengthy calculation and some approximations

$$\sigma^{qQ\to qQg} \approx \frac{2C_F \sigma^{qQ\to qQ}}{\pi} \int \frac{\mathrm{d}z}{1-z}\frac{\mathrm{d}Q^2}{Q^2}\alpha_s, \tag{6.6}$$

where $\sigma^{qQ\to qQ}$ is the leading order cross section for a massless quark q to scatter with a massive medium quark Q and the integral can be interpreted as the probability for medium induced gluon radiation.
The hadronization procedure is not modified since it is assumed that the hadronization takes place outside of the medium.

6.2 PYQUEN

In PYQUEN [24, 25], the accumulative energy loss was calculated in the BDMS framework and is subtracted from the parton energy in each scattering.
The integral equation for the energy loss as a function of the initial energy and the path length is given as

$$\Delta E(L,E) = \int_0^L \mathrm{d}l \frac{\mathrm{d}P(l)}{\mathrm{d}l}\lambda(l)\frac{\mathrm{d}E(l,E)}{\mathrm{d}l}, \qquad \frac{\mathrm{d}P(l)}{\mathrm{d}l} = \frac{1}{\lambda(l)}\exp(-l/\lambda(l)), \tag{6.7}$$

where l is the transverse coordinate of the parton, $\mathrm{d}P/\mathrm{d}l$ the scattering probability density and $\lambda = 1/(\sigma\rho)$ is the in-medium mean free path defined as reciprocal of the product of the integrated cross section σ and the medium density ρ. The collisional part of the energy

loss is defined as

$$\frac{\mathrm{d}E_{\mathrm{col}}}{\mathrm{d}l} = \frac{1}{4T\lambda\sigma}\int_{\mu_D^2}^{t_{\max}} \mathrm{d}t\,\frac{\mathrm{d}\sigma}{\mathrm{d}t}t \tag{6.8}$$

where the dominant contribution to the differential cross section is given as

$$\frac{\mathrm{d}\sigma}{\mathrm{d}t} \approx C_F\frac{2\pi\alpha_s^2(t)}{t^2}\frac{E^2}{E^2-m_q^2} \tag{6.9}$$

and the coupling constant is taken with one loop running coupling (2.3). The integration is regularized by the Debye mass and the maximal possible momentum transfer.
For the radiative energy loss, one finds

$$\frac{\mathrm{d}E_{\mathrm{rad}}}{\mathrm{d}l} = \frac{2\alpha_s(\mu_D^2)C_R}{\pi L}\int_{\omega_{\min}}^{E}\mathrm{d}\omega\left(1-y+\frac{y^2}{2}\right)\ln|\cos(\omega_1\tau_1)|, \tag{6.10}$$

$$\tag{6.11}$$

where

$$\omega_1 = \sqrt{\mathrm{i}\left(1-y+\frac{C_R}{3}y^2\right)\bar{\kappa}\ln\frac{16}{\bar{\kappa}}} \qquad \text{and} \qquad \bar{\kappa} = \frac{\mu_D^2\lambda_g}{\omega(1-y)}. \tag{6.12}$$

The spatio-temporal evolution of the medium is again described by the Bjorken model.
The gluon emission spectrum is also an input variable where the parametrization

$$\frac{\mathrm{d}N^g}{\mathrm{d}\theta} \propto \sin\theta\exp\left(-\frac{(\theta-\theta_0)^2}{2\theta_0^2}\right), \qquad \theta_0 \sim 5^\circ, \tag{6.13}$$

was used. But there is also the possibility to choose the wider gluon distribution $\mathrm{d}N^g/\mathrm{d}\theta \propto 1/\theta$.
The simulation starts each event with the generation of the initial parton spectrum with PYTHIA. Then the jet production vertex is produced at impact parameter b according to the distribution

$$\frac{\mathrm{d}^2N_{\mathrm{jet}}}{\mathrm{d}\phi\mathrm{d}r}(b) = \frac{T_A(r_1)T_A(r_2)}{\int_0^{2\pi}\mathrm{d}\phi\int_0^{R_{\max}} rT_A(r_1)T_A(r_2)\,\mathrm{d}r}, \tag{6.14}$$

where $r_{1,2}(b, r, \phi)$ are the distances between the nucleus centers and the jet production vertex V and $r_{\max}$ is the maximum possible transverse distance r from the beam axis to V. After this, the scattering cross section and transverse distance, $l_i = (\tau_{i+1} - \tau_i)E/p_T$, between scatterings is produced and the energy of each parton is reduced by sum collisional and radiative energy losses, $\Delta E_{\text{tot},i} = \Delta E_{\text{col},i} + \Delta E_{\text{rad},i}$. This parton rescattering is repeated until ether the parton escapes the dense zone, the QGP cools down below the critical temperature $T_c = 200\,\text{MeV}$ or the parton loses so much energy that its $p_T(\tau)$ drops below $2T(\tau)$. In the end, the hadronization is again done by PYTHIA.

7 Numerical Results

7.1 Jet Suppression in PbPb-Collisions

The two main observables for jet quenching are the jet modification factors R_{AA} and R_{CP}. The observable R_{AA} compares a heavy ion collision to proton-proton-collision with the same kinematics,

$$R_{AA} = \frac{\dfrac{1}{N_{\text{evt}}} \dfrac{\mathrm{d}^2 N_{AA}}{\mathrm{d}p_T \mathrm{d}\eta}}{\langle N_{\text{coll}} \rangle \dfrac{1}{N_{\text{evt}}} \dfrac{\mathrm{d}^2 N_{pp}}{\mathrm{d}p_T \mathrm{d}\eta}}, \tag{7.1}$$

where N_{coll} is averaged over the impact factor range and N_{AA}, respectively N_{pp} are the yield of jets as a function of rapidity η and transversal momentum p_T. This is then averaged over the total number of events that were measured.
If a heavy ion were just a loose collection of nucleons, one would expect $R_{AA} = 1$. Any observed deviation from unity can then be linked to the strongly interacting matter [6].
The other modification factor relates central collisions, where the impact factor is small to those collisions where the impact factor is large,

$$R_{CP} = \frac{\dfrac{1}{\langle T_{AA} \rangle} \dfrac{1}{N_{\text{evt}}} \dfrac{\mathrm{d}^2 N_{AA}}{\mathrm{d}p_T \mathrm{d}\eta}\Big|_{\text{central}}}{\dfrac{1}{\langle T_{AA} \rangle} \dfrac{1}{N_{\text{evt}}} \dfrac{\mathrm{d}^2 N_{AA}}{\mathrm{d}p_T \mathrm{d}\eta}\Big|_{\text{peripheral}}}. \tag{7.2}$$

Usually a collision is considered to be central, if the centrality lies below 50 % and otherwise it is peripheral. In the peripheral case most nucleons are not taking part in the collision

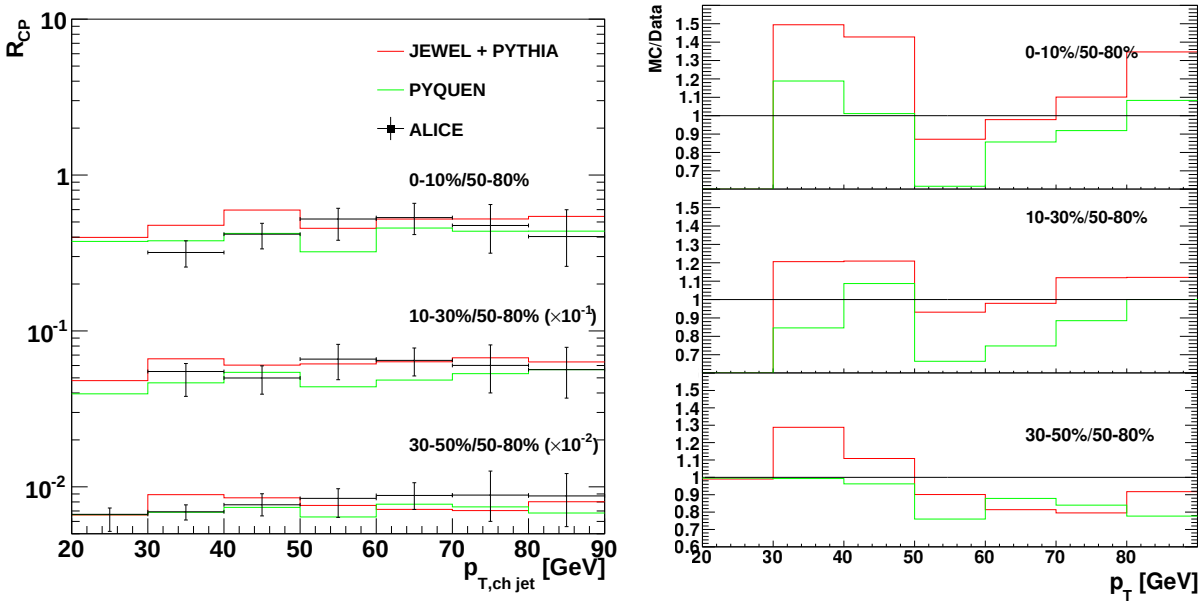

Figure 7: On the left, the simulation results for the central to peripheral ratio R_{CP} for charged jets is shown for $\sqrt{s} = 2760\,\text{GeV}$ compared to ALICE data [26] for jet radius $R = 0.2$. On the right side, the ratios between Monte Carlo results and experiment are shown for better comparison.

so less QGP will be formed and jets are expected to experience less suppression.
Both observables depend on the center of mass energy, the jet algorithm and jet radius and on the detector and its geometry, i.e. what solid angle is covered and what kinds of particles can be measured.
In the figures 7 - 10 the numerical results for both observables from JEWEL and PYQUEN are compared to measurements from the ALICE experiment at the LHC.
For R_{CP} both models are in good agreement to the experiment while for R_{AA} PYQUEN seems to give slightly better results although the JEWEL results are also in quite good agreement.

7.2 Parameter dependence of the simulations

In the figures 11 - 18 some parameters were varied with the other parameters, respectively, being left unchanged. The default parameters are shown in appendix B. The results for JEWEL and PYQUEN are shown in different plots to not overload the figures. In the PYQUEN plots the label "wide" corresponds to a wider angular distribution for the gluon emissions as in section 6.2 discussed. The variable T_0 corresponds to the mean initial tem-

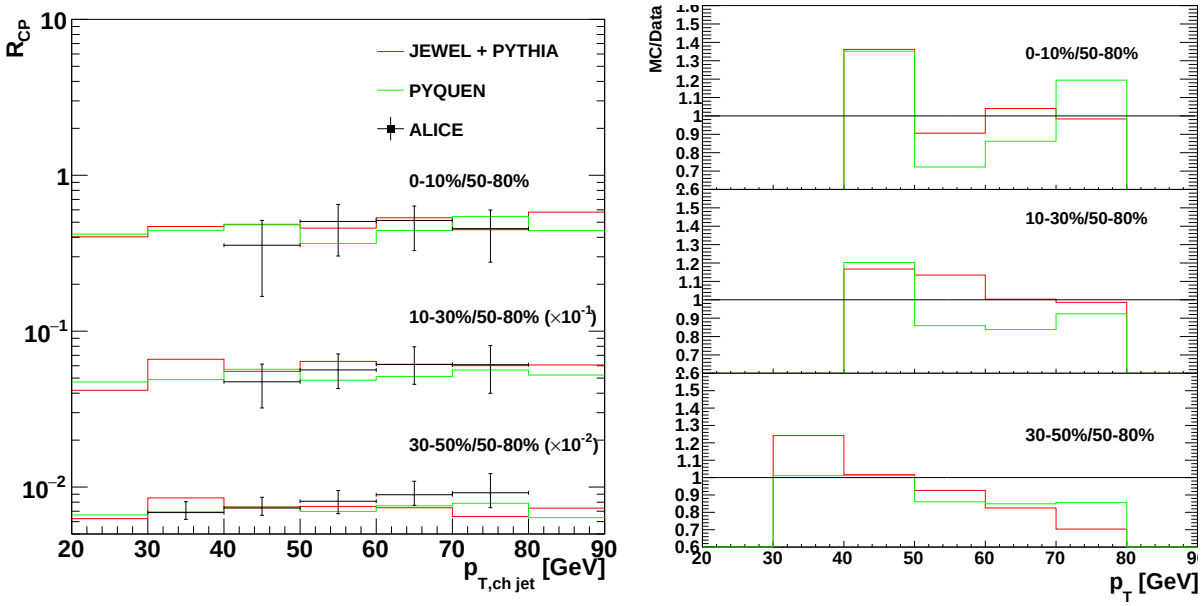

Figure 8: On the left, the simulation results for the central to peripheral ratio R_{CP} for charged jets is shown for $\sqrt{s} = 2760\,\text{GeV}$ compared to ALICE data [26] for jet radius $R = 0.3$. On the right side, the ratios between Monte Carlo results and experiment are shown for better comparison.

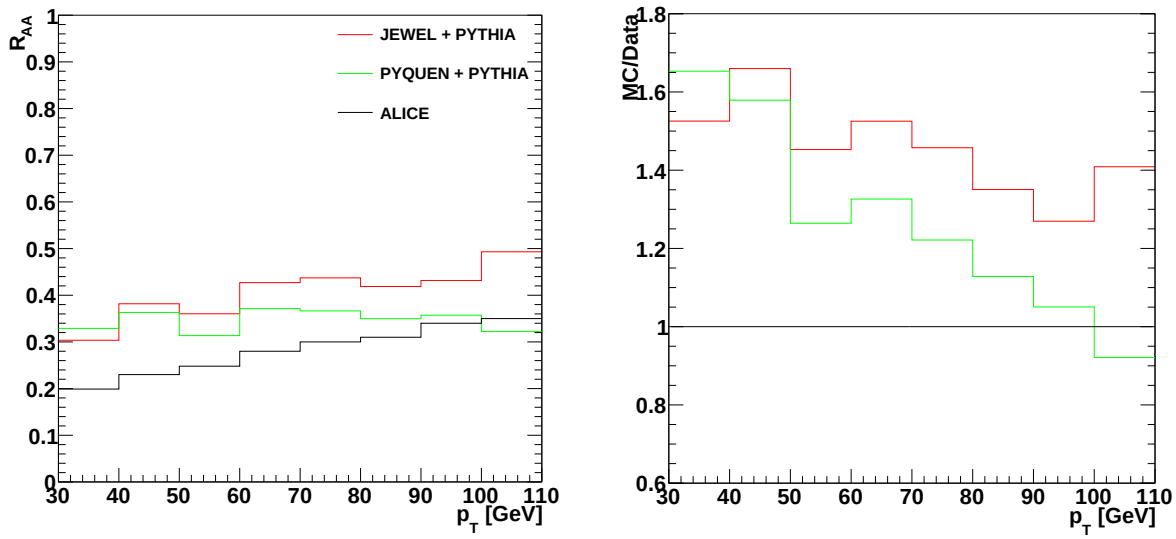

Figure 9: On the left, the simulation results for the central to peripheral ratio R_{AA} for charged jets is shown for $\sqrt{s} = 2760\,\text{GeV}$ compared to ALICE data [27] for jet radius $R = 0.2$ and $0 - 10\%$ centrality. On the right side, the ratios between Monte Carlo results and experiment are shown for better comparison. The experimental data points were read off the plots.

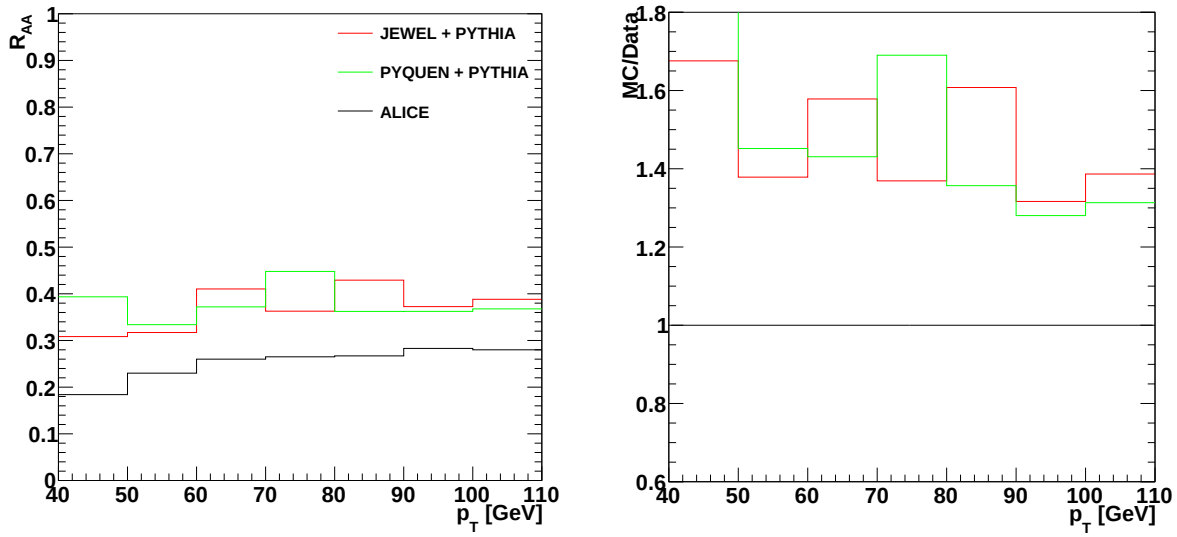

Figure 10: On the left, the simulation results for the central to peripheral ratio R_{AA} for charged jets is shown for $\sqrt{s} = 2760\,\text{GeV}$ compared to ALICE data [27] for jet radius $R = 0.3$ and $0 - 10\%$ centrality. On the right side, the ratios between Monte Carlo results and experiment are shown for better comparison. The experimental data points were read off the plots.

perature while it corresponds to the maximum initial temperature in PYQUEN.

8 Conclusion

In this thesis the two Monte Carlo models JEWEL and PYQUEN were presented and compared to experimental results from ALICE. For that matter, the foundations of perturbative QCD, especially the basics of parton showers and hadronization, reviewed.
It was shown that both models are in quite good agreement with the experiment

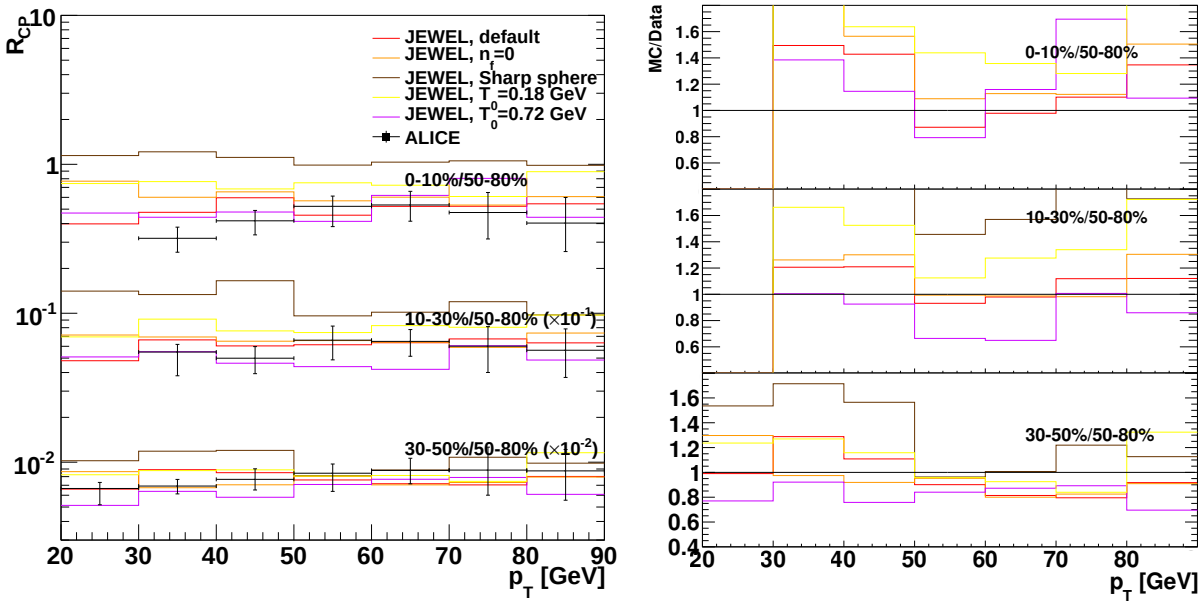

Figure 11: On the left, the simulation results for the central to peripheral ratio R_{CP} for charged jets is shown for $\sqrt{s} = 2760\,\text{GeV}$ compared to ALICE data [26] for jet radius $R = 0.2$. One medium parameter was varied, compared to the default configuration in JEWEL. On the right side, the ratios between Monte Carlo results and experiment are shown for better comparison.

Appendix

A Monte Carlo methods

A.1 Basic Monte Carlo integration

In almost all calculations in particle physics one has to integrate over a multi-dimensional phase space to get some final result, which usually has to be done numerically.
When using classical integration techniques, such as the Trapezoidal or the Simpson rule, the convergence rate decreases with the dimension of the integral [8] while the convergence of the Monte Carlo (MC) method is independent of the dimension as will be shown later. The basic idea of MC is to express an integration by the mean value of the considered function,

$$I[f] = \int_V f(x)\mathrm{d}^n x \approx V\langle f\rangle, \qquad \text{where} \qquad \langle f\rangle = \frac{1}{N}\sum_{i=1}^{N} f(x_i). \tag{A.1}$$

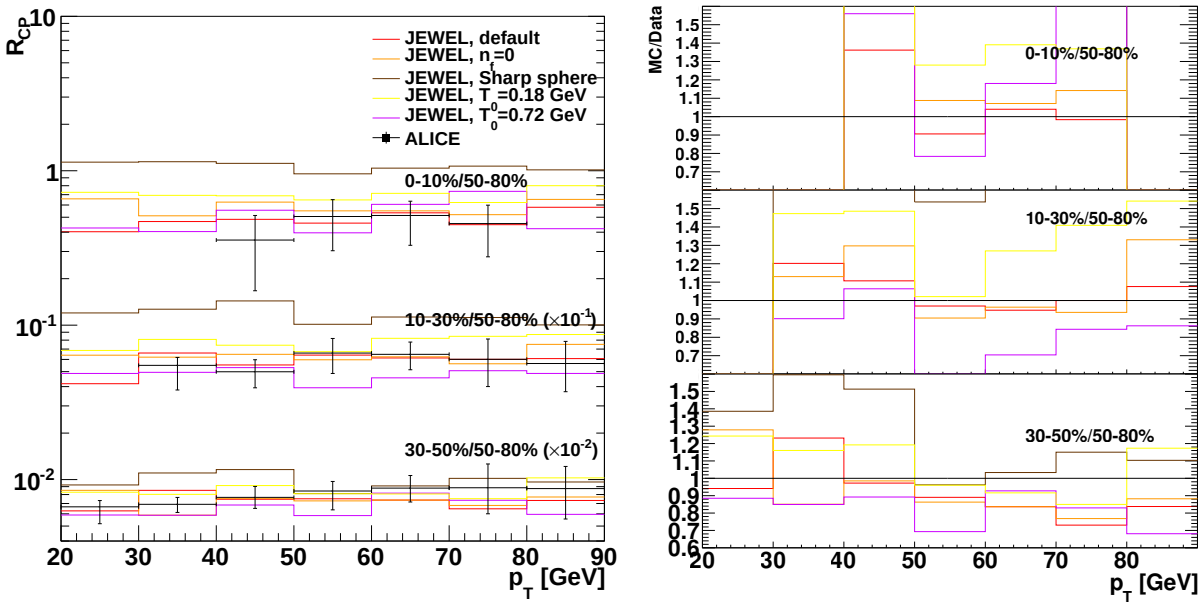

Figure 12: On the left, the simulation results for the central to peripheral ratio R_{CP} for charged jets is shown for $\sqrt{s} = 2760\,\text{GeV}$ compared to ALICE data [26] for jet radius $R = 0.3$. One medium parameter was varied, compared to the default configuration in JEWEL. On the right side, the ratios between Monte Carlo results and experiment are shown for better comparison.

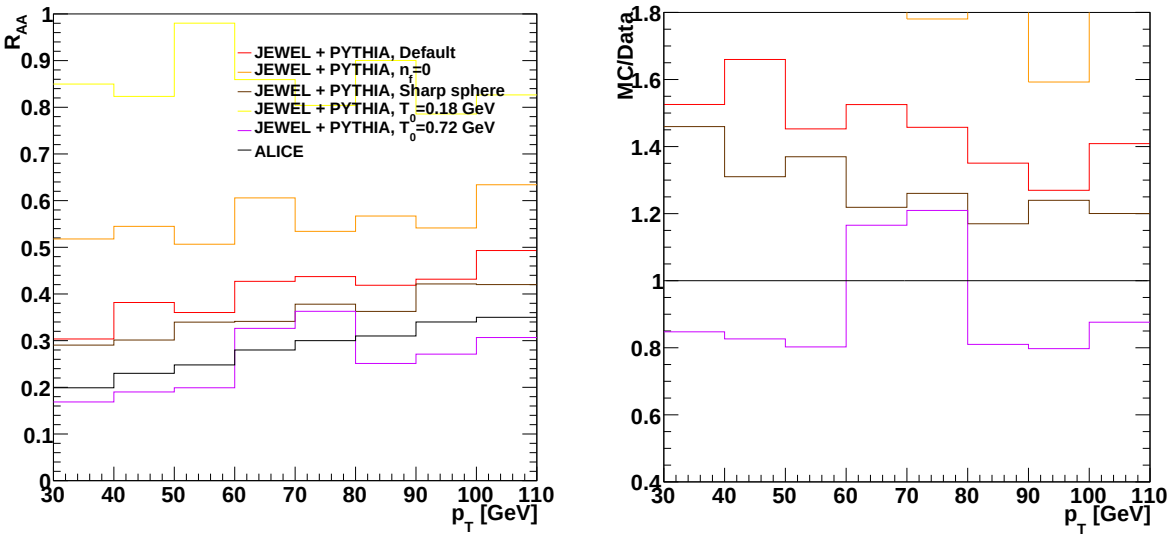

Figure 13: On the left, the simulation results for the central to peripheral ratio R_{AA} for charged jets is shown for $\sqrt{s} = 2760\,\text{GeV}$ compared to ALICE data [27] for jet radius $R = 0.2$ and $0 - 10\%$ centrality. One medium parameter was varied, compared to the default configuration in JEWEL. On the right side, the ratios between Monte Carlo results and experiment are shown for better comparison. The experimental data points were read off the plots.

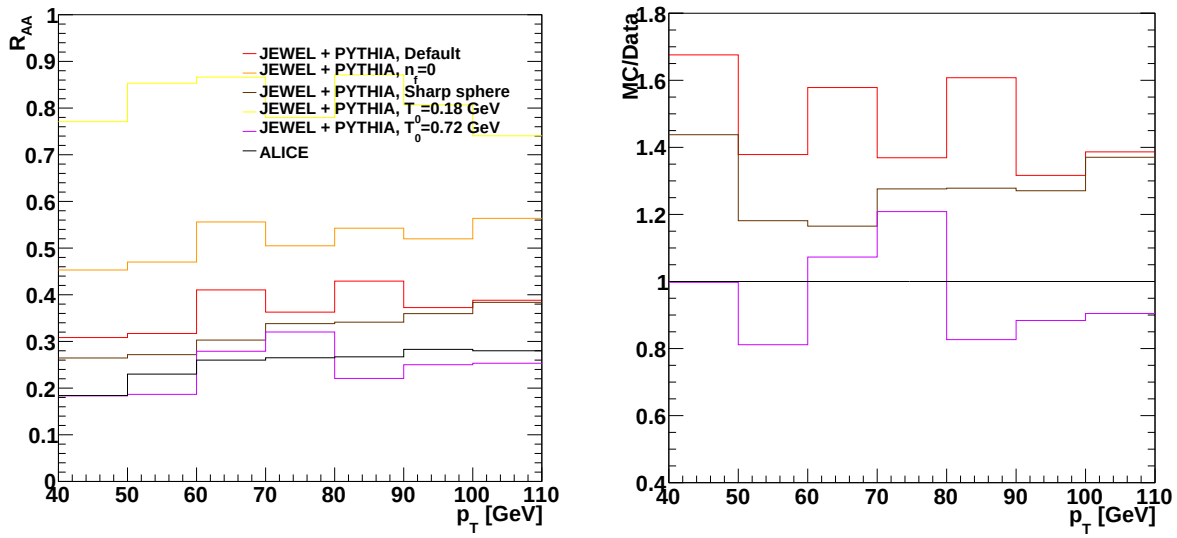

Figure 14: On the left, the simulation results for the central to peripheral ratio R_{AA} for charged jets is shown for $\sqrt{s} = 2760\,\text{GeV}$ compared to ALICE data [27] for jet radius $R = 0.3$ and $0 - 10\%$ centrality. One medium parameter was varied, compared to the default configuration in JEWEL. On the right side, the ratios between Monte Carlo results and experiment are shown for better comparison. The experimental data points were read off the plots.

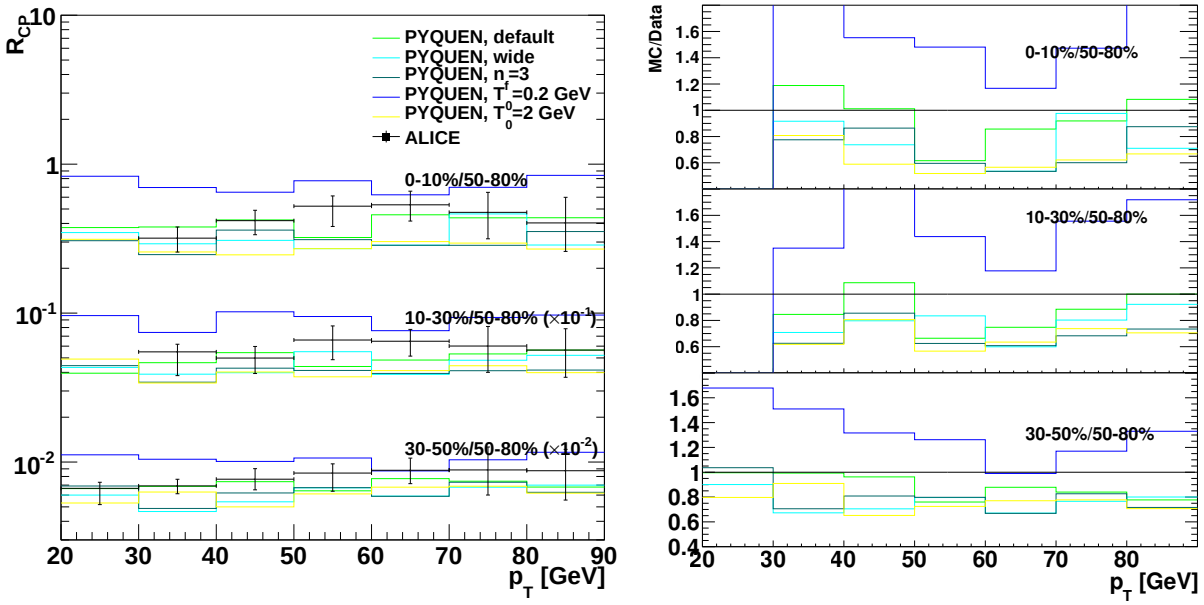

Figure 15: On the left, the simulation results for the central to peripheral ratio R_{CP} for charged jets is shown for $\sqrt{s} = 2760\,\text{GeV}$ compared to ALICE data [26] for jet radius $R = 0.2$. One medium parameter was varied, compared to the default configuration in PYQUEN. On the right side, the ratios between Monte Carlo results and experiment are shown for better comparison.

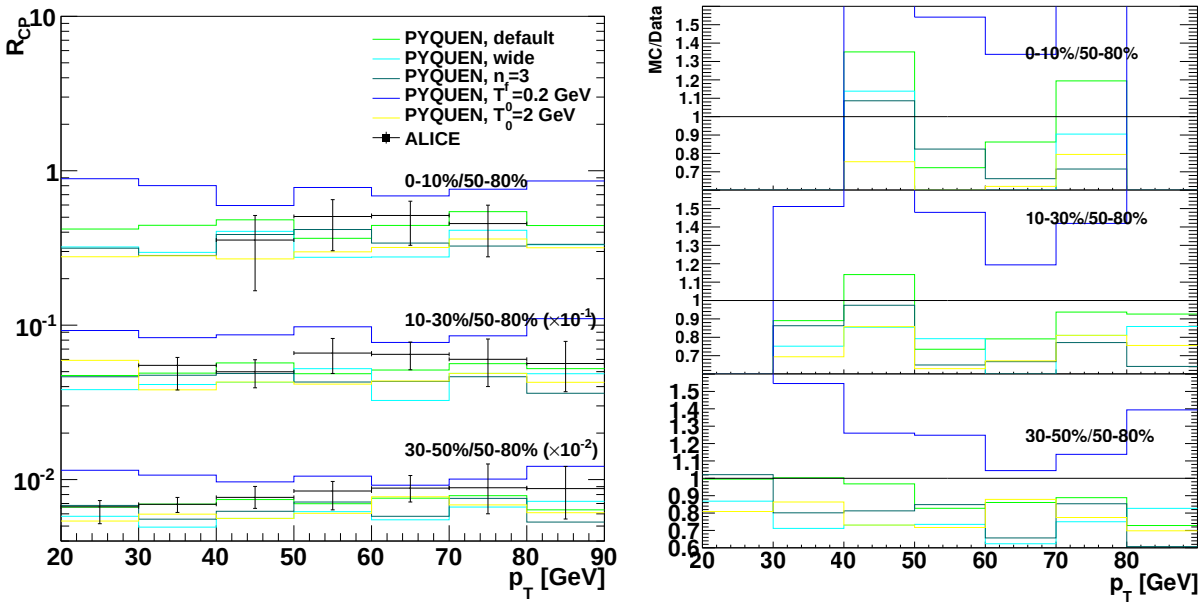

Figure 16: On the left, the simulation results for the central to peripheral ratio R_{CP} for charged jets is shown for $\sqrt{s} = 2760\,\text{GeV}$ compared to ALICE data [26] for jet radius $R = 0.3$. One medium parameter was varied, compared to the default configuration in PYQUEN. On the right side, the ratios between Monte Carlo results and experiment are shown for better comparison.

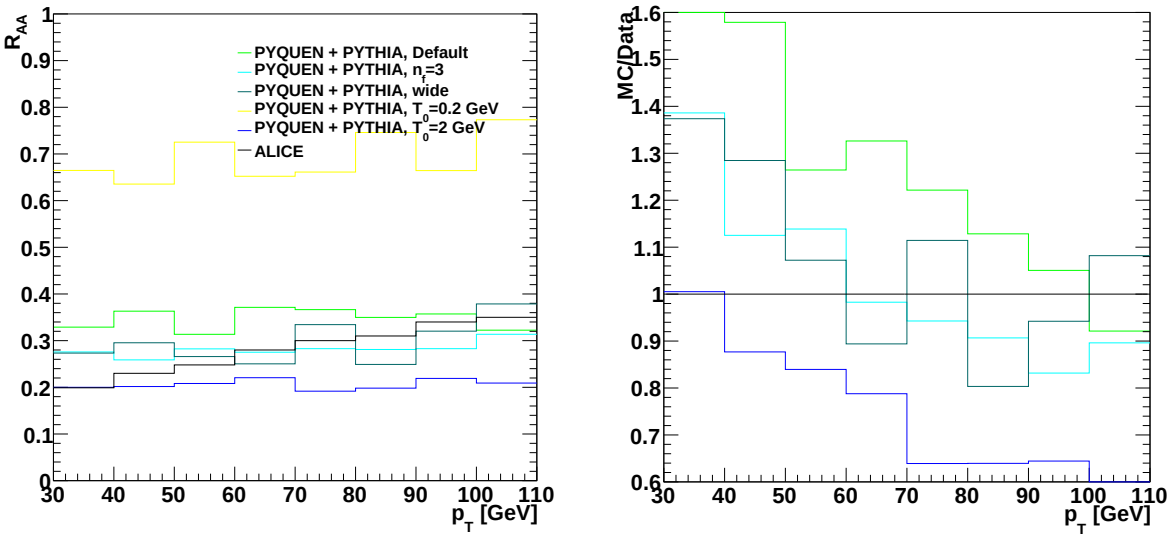

Figure 17: On the left, the simulation results for the central to peripheral ratio R_{AA} for charged jets is shown for $\sqrt{s} = 2760\,\text{GeV}$ compared to ALICE data [27] for jet radius $R = 0.2$ and $0 - 10\%$ centrality. One medium parameter was varied, compared to the default configuration in PYQUEN. On the right side, the ratios between Monte Carlo results and experiment are shown for better comparison. The experimental data points were read off the plots.

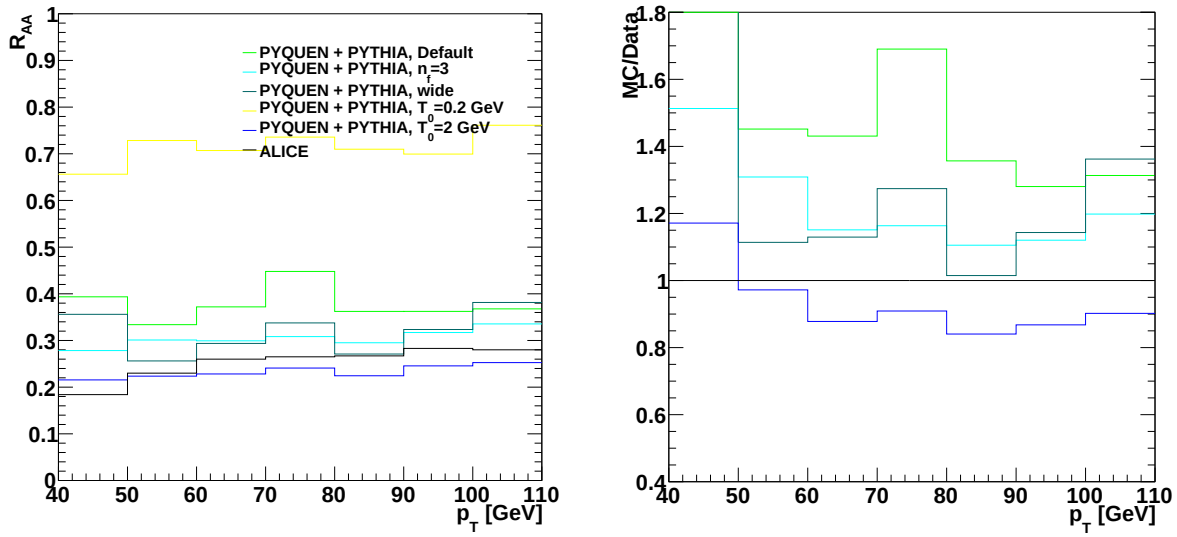

Figure 18: On the left, the simulation results for the central to peripheral ratio R_{AA} for charged jets is shown for $\sqrt{s} = 2760\,\text{GeV}$ compared to ALICE data [27] for jet radius $R = 0.3$ and $0 - 10\%$ centrality. One medium parameter was varied, compared to the default configuration in PYQUEN. On the right side, the ratios between Monte Carlo results and experiment are shown for better comparison. The experimental data points were read off the plots.

If the points x_i are distributed randomly and uniformly over the volume V, the expression on the right hand side will converge to the integral by means of the central limit theorem [8]. The estimated error $E[f]$ is given by

$$E[f] = \sqrt{\frac{\langle f^2 \rangle - \langle f \rangle^2}{N-1}}, \tag{A.2}$$

which is independent of the dimensionality of the problem, but depends only on the variance of the integrand f in the numerator.

A.2 Variance Reduction

The simple integration procedure from the previous section samples every subset of the volume V with the same probability. This means that subsets where f vanishes or is very small und thus do not contribute much or anything to the sum in (A.1) will in principle be sampled as often as subsets where f is large. To circumvent this let g be a function with $g(x) \neq 0$ for all $x \in V$ such that f/g has a lower variance than f and $g(x)\mathrm{d}^n x$ is an exact

differential form then (A.1) can be rewritten as

$$I[f] = \int_V \frac{f(x)}{g(x)} g(x) \mathrm{d}^n x. \tag{A.3}$$

However, the integration process in (A.3) can be interpreted as sampling $h = f/g$ over the nonuniform probability density $\mathrm{d}^n\mu(x) = g(x)\mathrm{d}^n x$ [28]. This interpretation is then used in for example in the VEGAS MC algorithm where the integrand is first sampled uniformly for a comparatively low number of times to find a probability distribution that is well-suited for the integrand and then this density is used to integrate the function taking into account where its maxima and minima are.

B Default parameters in the simulations

B.1 JEWEL

Table 1: Default medium parameters in JEWEL [22]

Parameter	Variable	Default value
Initial time τ_i [fm]	`TAUI`	0.6
Mean initial temperature T_i [GeV]	`TI`	0.36
Woods-Saxon potential?	`WOODSSAXON`	T ("True")
Lower end of centrality range [%]	`CENTRMIN`	0
Upper end of centrality range [%]	`CENTRMAX`	10
Number of flavors in the QGP	`NF`	3
Mass number of colliding nuclei	`A`	208
Density parameter of Woods-Saxon potential [fm^{-3}]	`NO`	0.17
Thickness parameter of Woods-Saxon potential [fm]	`D`	0.54
Nucleon-nucleon cross section [fm^2]	`SIGMANN`	6.2
Minimum of infra-red regulator [GeV]	`MDFACTOR`	0.45
Factor multiplying to the infra-red regulator, i.e. $\mu_D = 3T$	`MDSCALEFAC`	0.9

B.2 PYQUEN

Table 2: Default medium parameters in PYQUEN [29]

Parameter	Variable	Default value
Maximum initial temperature [GeV]	`T0`	1
Proper time of QGP formation [fm]	`tau0`	0.1
Number of flavors in the QGP	`nf`	0
Energy loss mechanisms	`ienglu`	0
Angular distribution of emitted gluons	`ianglu`	0

- The variable `ienglu` is enumerating the options "radiative & collisional energy loss", "radiative energy loss only" and "collisional energy loss only" from 0 to 2.
- The variable `ianglu` is enumerating the options "small-angular", "wide-angular" and "collinear" from 0 to 2.

References

[1] T. Boeckel, J. Schaffner-Bielich, arXiv:1105.0832 [astro-ph.CO].

[2] P. Skands, arXiv:1207.2389v2 [hep-ph].

[3] M. Kaku, "Quantum Field Theory: A Modern Introduction". Oxford University Press, 1993.

[4] G. Sterman et al., Rev. Mod. Phys. 67, 157, 1995.

[5] L. Ryder, "Quantum Field Theory". Cambridge University Press, 1996.

[6] D. d'Enterria, arXiv:0902.2011 [nucl-ex].

[7] G. Salam, arXiv:0906.1833 [hep-ph].

[8] A. Buckley et al., arXiv:1101.2599 [hep-ph].

[9] G. Salam, G. Soyez, arXiv:0704.0292 [hep-ph].

[10] M. Cacciari, G. Salam, G. Soyez, arXiv:1111.6097 [hep-ph].

[11] Y. Dokshitzer et al., "Basics of Perturbative QCD". Editions Frontieres, 1991.

[12] T. Sjostrand, S. Mrenna, P. Skands, arXiv:hep-ph/0603175.

[13] B. Andersson, G. Gustafson, T. Sjostrand, Nuc. Phys. B197 (1982) 45-54.

[14] K. Zapp, "A Monte Carlo Model for Jet Evolution With Energy Loss". Dissertation Uni Heidelberg, 2008.

[15] J. Ollitrault, arXiv:0708.2433 [nucl-th].

[16] J. Bjorken, Phys. Rev. D 27 (1983) 140-151.

[17] L. Csernai, "Introduction to Relativistic Heavy Ion Collisions". John Wiley & Sons Ltd, 1994.

[18] M. Miller et al., arXiv:nucl-ex/0701025.

[19] T. Plehn, arXiv:0910.4182 [hep-ph].

[20] K. Zapp, F. Krauss, U.Wiedemann, arXiv:1212.1599 [hep-ph].

[21] K. Zapp et al., arXiv:hep-ph/0512300.

[22] K. Zapp, arXiv:1311.0048 [hep-ph].

[23] K. Zapp et al., arXiv:0804.3568 [hep-ph]

[24] I. Lokhtin, A. Snigirev, arXiv:hep-ph/0406038.

[25] I. Lokhtin, A. Belyaev, A. Snigirev, arXiv:1103.1853 [hep-ph].

[26] ALICE Collaboration, arXiv:1311.0633 [nucl-ex].

[27] M. Verweij, arXiv:1208.6169 [nucl-ex].

[28] W. Press et al., "Numerical Recipes in C". Cambridge University Press, 1992.

[29] PYQUEN-README, http://lokhtin.web.cern.ch/lokhtin/pyquen/pyquen.txt (last time visited: 26.12.2014)

Eigenständigkeitserklärung

Hiermit versichere ich, dass die vorliegende Arbeit *Comparison of Jet Quenching mechanisms in heavy ion collisions* (deutscher Titel: *Vergleich von Jet-Quenching-Modellen in Schwerionenkollisionen*) selbstständig verfasst worden ist, dass keine anderen Quellen und Hilfsmittel als die angegebenen benutzt worden sind und dass die Stellen der Arbeit, die anderen Werken – auch elektronischen Medien – dem Wortlaut oder Sinn nach entnommen wurden, auf jeden Fall unter Angabe der Quelle als Entlehnung kenntlich gemacht worden sind.

Münster, den January 22, 2015 _____

Semir Vrana

Ich erkläre mich mit einem Abgleich der Arbeit mit anderen Texten zwecks Auffindung von Übereinstimmungen sowie mit einer zu diesem Zweck vorzunehmenden Speicherung der Arbeit in eine Datenbank einverstanden.

Münster, den 29.12.2014 _____

Semir Vrana